P. LACKI*, A. DERLATKA*,#

THE PLASTIC DEFORMATION OF RFSSW JOINTS DURING TENSILE TESTS

DEFORMACJA PLASTYCZNA WYBRANYCH POŁĄCZEŃ RFSSW PODCZAS ROZCIĄGANIA

The dynamic development of the friction stir welding (FSW) technology is the basis for the design of durabe joints inter alia in the aviation industry. This technology has a prospective application, especially for the aluminum alloys. It is suitable for a broad spectrum of permanent joints. The joints obtained by FSW technology are characterized by good mechanical properties. In this paper, the friction stir spot welding joints were analysed. The example of a structure made using this technology were presented. The lap joints made of 2mm Al 6061-T6 sheets were the investigation subject. The different spot welds arrangements were analysed. The tensile test were performed with optical deformation measurement system, which allow to obtain the plastic deformation field on the sample surface. The plastic strain graphs for the characteristic line passing through the maximum deformation were registered and presented. The experimental results were compared to the FEM numerical analysis. The numerical models were built with 3D-solid elements. The boundary conditions, material properties and geometry of the joints were identical as during experimental investigation. The mechanism of deformation of welded joints during tensile test was described and explained. It has been found that the arrangement of the spot welds with respect to the tensile direction has an important influence on the behaviour and deformation of lap joint.

Dynamiczny rozwój technologii zgrzewania tarciowego z mieszaniem (FSW) jest podstawą do projektowania wytrzymałych połączeń między innymi w przemyśle lotniczym. Technologia ta, szczególnie dla stopów aluminium, ma perspektywiczne zastosowanie. Nadaje się do wykonywania szerokiego spektrum połączeń nierozłącznych. Połączenia uzyskane przy użyciu tej technologii cechują się dobrymi właściwościami mechanicznymi i użytkowymi. W pracy analizowano połączenia uzyskane przy użyciu technologii punktowego zgrzewania tarciowego z mieszaniem (RFSSW). Zaprezentowano przykład elementu konstrukcji wykonanej przy użyciu tej technologii. Przedmiotem badań w pracy były połączenia zakładkowe wykonane z 2mm blachy Al 6061-T6. Połączenia zgrzewane różniły się ułożeniem zgrzein punktowych. Próbki rozciągano na maszynie wytrzymałościowej, jednocześnie dokonując pomiaru przy użyciu optycznego systemu pomiaru deformacji. Przy użyciu tego systemu uzyskano pole odkształceń plastycznych na powierzchni rozciąganej próbki. Zarejestrowano i przedstawiono wykresy odkształceń plastycznych dla charakterystycznych linii przechodzących przez maksimum odkształcenia. Wyniki badań doświadczalnych odniesiono do przeprowadzonej analizy numerycznej MES. Model numeryczny zbudowano z elementów typu 3D solid. W modelu odwzorowano warunki brzegowe przeprowadzonej próby, właściwości materiału i geometrię złącza. Opisano i wyjaśniono mechanizm deformacji złącz zgrzewanych podczas rozciągania. Stwierdzono, że położenie zgrzein w stosunku do kierunku rozciągania ma istotny wpływ na pracę i deformację połączenia zakładkowego.

1. Introduction

During refill friction stir spot welding (RFSSW) process material is being stirred in its plastic state. The plasticization is produced by a specially designed tool (Fig. 1). The rotary tool movements and the resulting friction heat the base material, thus the probe can be plunged into the workpieces at the point of the forming joint. The material pushed out by the probe lifts the sleeve and fills the spaces previously occupied the sleeve (Fig. 2b). The final spot joint is formed after the probe has been lifted and the sleeve has been lowered (Fig. 2c) [1–3].
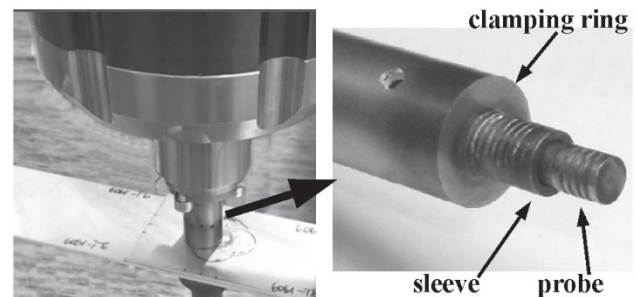

Fig. 1. Tool for RFSSW process

* CZESTOCHOWA UNIVERSITY OF TECHNOLOGY, 69 DĄBROWSKIEGO STR., 42-200 CZĘSTOCHOWA, POLAND

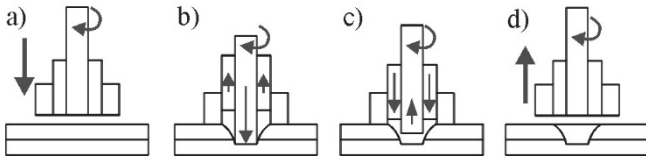# Corresponding author: aderlatka@bud.pcz.czest.pl

Fig. 2. Stages of RFSSW process: a) tool positioning, b) plunged probe, c) plunged sleeve, d) tool retraction

RFSSW is mainly used for joining aluminum alloys components. The papers [4, 5] present the possibilities of using this technology for welding steel as well as titanium with aluminum.

In the RFSSW, the surface of the spot face is smooth, no element protrudes above the sheets top surfaces, and the duration of the process is shorter than in case of the riveting, as presented in [6]. [7–9] show that RFFSW belongs to the state-of-the-art joining technologies due to the high strength of the spot welds and the simplicity of the process performance.

In the paper [10] the load-capacity and microstructure of the RFSSW joints made of aluminium alloy 6061-T4 were presented. Also the characteristics of the hooks and voids made at different processing parameters were discussed. The authors of the paper [11, 12] analyzed the influence of 15 parameters combination on the mechanical properties and microstructure of the RFSSW joints made of aluminium alloy 6181-T6 with a thickness of 1.7 mm. The analysis of the joints made of aluminum alloy 7xxx was shown in [13]. Whereas studies of RFSSW joints made of aluminum alloy 2xxx were presented in [14].

The technology is used in the automotive and aerospace industries, for instance in the panel structures and in the load-bearing constructions (Fig. 3) analysed in [15–17].
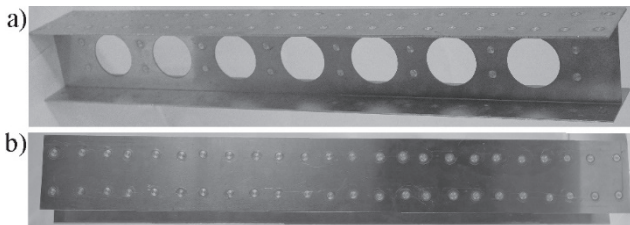

Fig. 3. Load-bearing structure made by RFSSW: a) axonometric view, b) top view

The modelling of RFSSW process and structures produced by RFSSW is still being developed. The thermo-mechanical models are used for the analysis of the welding process. The heat source distributed over the contact surface of the tool is modelled as a heat flux loading the surface of the upper sheet. The analysis of normal stresses and temperature distributions for varying welding parameters (welding speed, rotational speed) were shown in [18, 19]. The mechanical models are used for the analysis of the structures made using RFSSW. These model apply different material properties for different volumes of the analysed material. The division into two groups: the base material and the spot with heat-affected zone (HAZ) is shown in [20]. In [21], four groups were defined: the spots, the thermo mechanically affected zone (TMAZ), the HAZ and the base material.

2. Goal and scope of work

The goal of the paper is to determine the crack locations in RFSSW joints during the tensile test. The assessment was made using experimental research and numerical analysis. Three types of overlap joint geometries were analysed. The joint were made of 2-mm thick 6061-T6 aluminium alloy sheets and were joined using two spot welds. Fig. 4 - 6 show the views of the specimens from the tool operation side – the obverse and from the opposite side – the reverse. For each geometry, the tests were performed using the series consisting of three specimens. The chemical composition of the base material is given in Table 1. The RFSSW process was performed using following: thickness of the spot of 2.2mm, tool rotational speed of 2000 rpm, tool input time of 0.7 s, tool output time of 0.5 s. The diameter of the weld spots was 9mm.
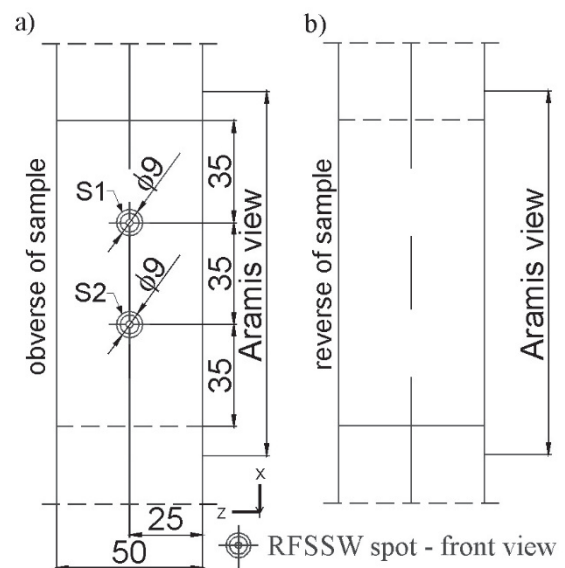

Fig. 4. Geometry of specimen with parallel spot welds: a) obverse view, b) reverse view
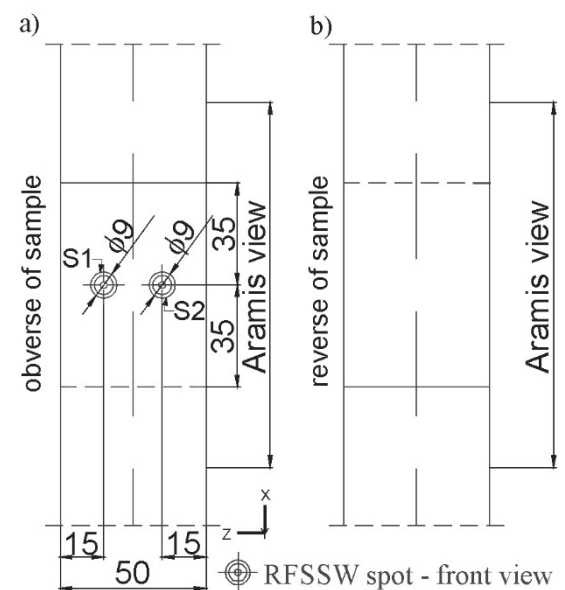

Fig. 5. Geometry of specimen with perpendicular spot welds : a) obverse view, b) reverse view
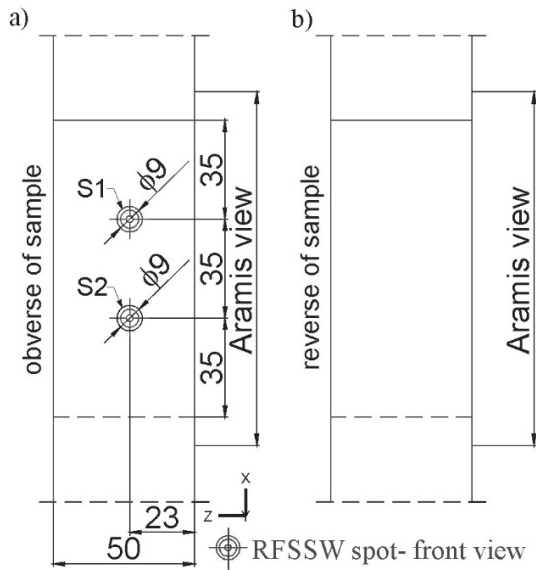
Fig. 6. Geometry of specimen with eccentrical, parallel spots : a) obverse view, b) reverse view

Tab. 1.

The joints were extended in the testing machine. A non-contact optical 3D deformation measurement system Aramis was applied. The use of Aramis system allowed for acquisition of effective plastic strain fields at the external surfaces of the extended specimens. The graphs of effective plastic strains for the characteristic lines passing through the maximum strains were recorded and presented. The results of the experimental investigations were compared with the numerical analyses carried out using ADINA System based on FEM.

3. Experimental investigation

The maximum forces achieved by the joints during the tensile tests were shown in the displacement-force graphs (Fig. 7). The maximum values of forces achieved by the joints are similar. The significant difference occurs for the joint with weld spots situated parallel, eccentrically to the tensile direction, the achieved displacement is almost twice greater than in case of the other joints.
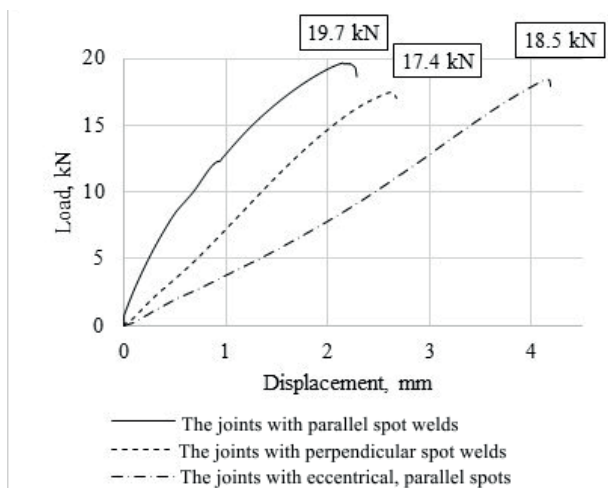

Fig. 7. Displacement-force diagram for analysed joints

The photos of the joints after stretching are shown in Fig. 8 - 9. The free ends of the specimens sheets with parallel spots, both axial and eccentrical, are slightly deflected with respect to the Y-axis. The joints are slightly deformed in the areas of the spot welds. The joints were destroyed by shearing at the spot welds. In the specimen with perpendicular spot welds, the free ends of the sheets are significantly deflected with respect to the Y-axis. The losing of joints load capacity is caused by the cracks occurring at the edges of the spot welds, at the side corresponding to the fixed sheet ends. The spot welds were not destroyed, they were only partially separated from the joints.
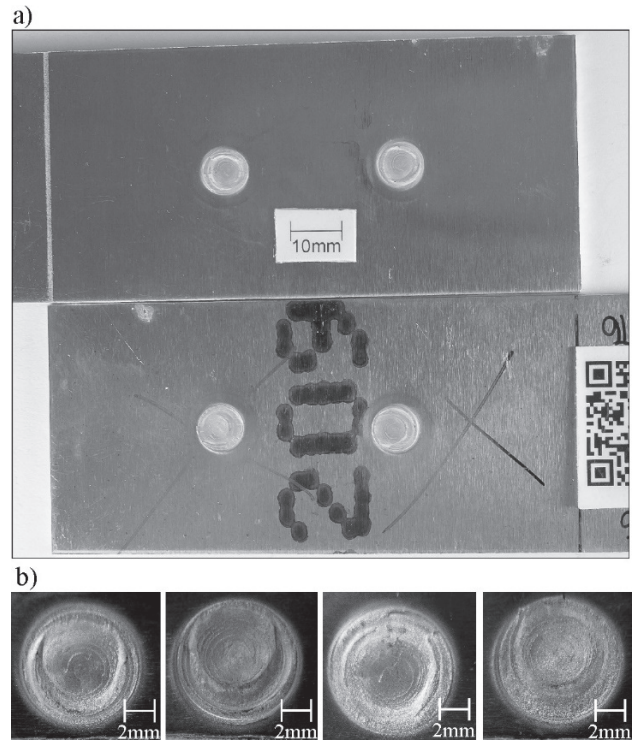

Fig. 8. Specimen with parallel spot welds after tensile test: a) view of destroyed joint, b) view of destroyed spot welds
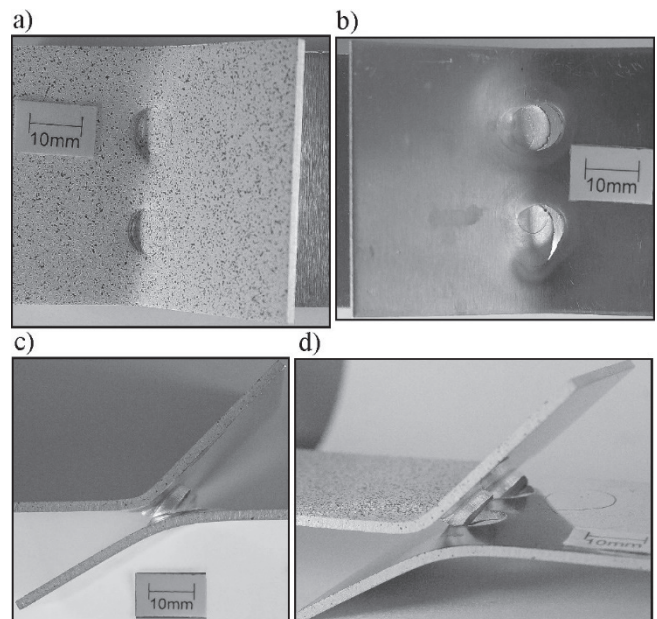

Fig. 9. Specimen with perpendicular spot welds after tensile test: a) obverse view, b) reverse view, c) side view, d) axonometric view

Chemical composition of 6061-T6 aluminium alloy

Element content, % wt.									
Cr	Cu	Fe	Mg	Mn	Si	Ti	Zn	other	Al
0.04-0.35	0.15-0.40	0.70	0.80-1.20	0.15	0.40-0.80	0.15	0.25	0.15	rest

The effective plastic strain distributions at the joints surfaces, at the time corresponding to achieving the maximum tensile forces, were shown in Fig. 10 - 12. In each joint, the effective plastic strains reach have higher values at the obverse surface of the specimen than at the reverse surface. In the specimens with parallel spot welds and with perpendicular spot welds, the effective plastic strain distributions are symmetrical with respect to the X-axis. In the joints with parallel spot welds, the higher effective plastic strains occur in the S1 spot welds. Two areas of effective plastic strain concentrations occur in the vicinity the S1 spot weld: corresponding to the highest and the lowest values at X-axis. The maximum values occur in the area corresponding to the lowest X value. In the joint with perpendicular spot welds, the zones of effective plastic strains concentrations occur at the edges of the spot welds (in the lower and external parts) and in the areas below the spot welds.

Fig. 11. Results of optical deformation analysis system - effective plastic strain distribution at the surface of specimen with perpendicular spot welds: a) obverse view, b) reverse view

The joints with eccentrical, parallel spots to the displacement direction the effective plastic strain distribution is asymmetrical with respect to the X-axis. The areas of effective plastic strains concentrations occur at the edge of S2 spot, at the points corresponding to the lowest X-values. Based on the analysis of effective plastic strain distribution with respect to the X-axis in the base material surrounding spot weld (obverse view), it can be seen that the higher values are at the right side.
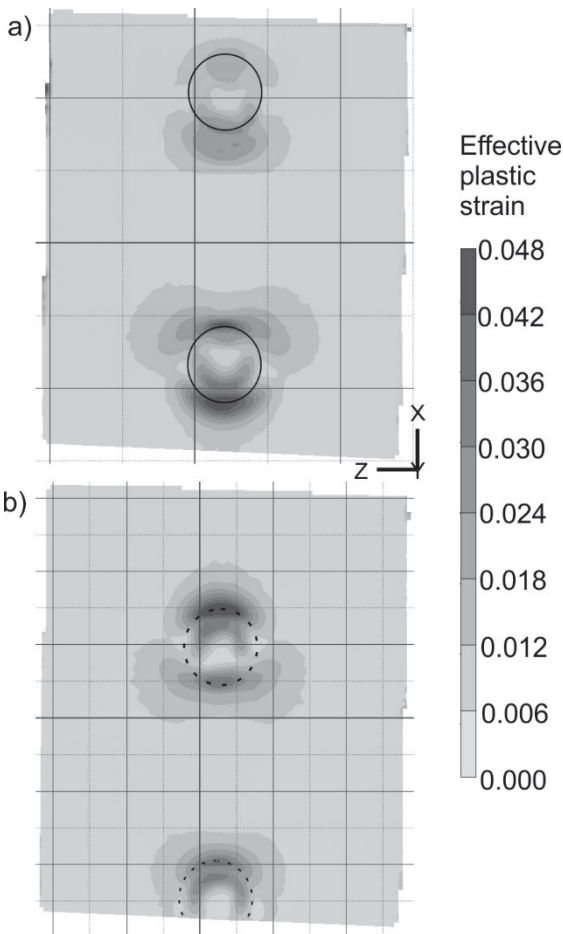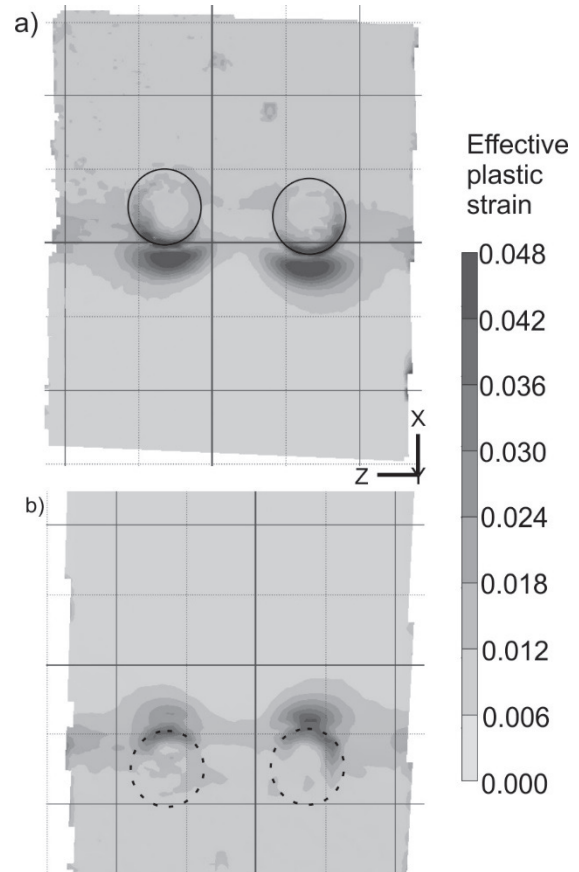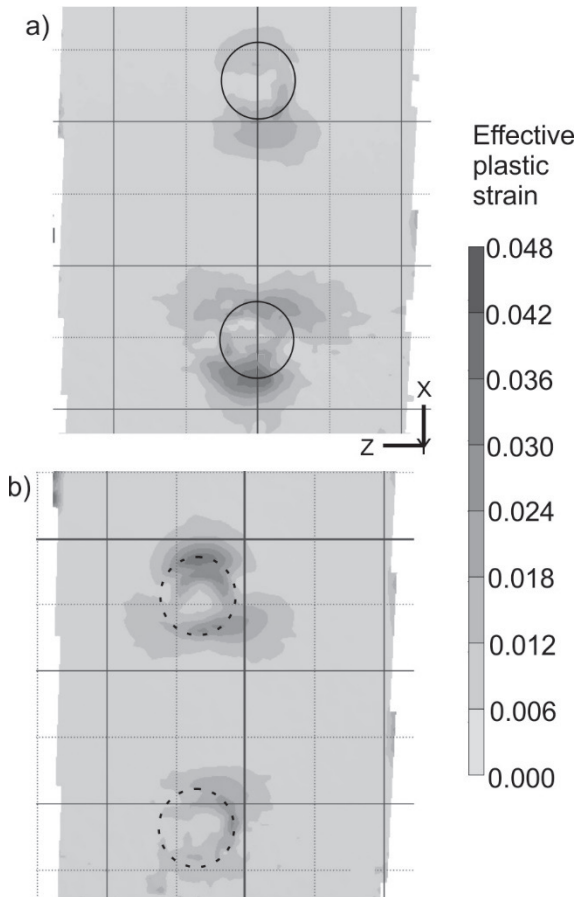

Fig. 10. Results from optical deformation analysis system - effective plastic strain distribution at the surface of specimen with parallel spot welds : a) obverse view, b) reverse view

Fig. 12. Results of optical deformation analysis system - effective plastic strain distribution at the surface of specimen with eccentrical, parallel spots: a) obverse view, b) reverse view

4. Numerical studies

The numerical studies were carried out with the ADINA System based on the finite element method. The spot welds and base material were modelled as 3D-solid elements. Between the 3D-solid element surfaces of the sheets, the contact conditions were assumed. The boundary conditions and type of load were the same for each specimen: the one external edge of the specimen was fixed, the second external edge of the specimen had one free degree of freedom (X-translation) and that edge was loaded by displacement. The values of loads equivalent to the maximum displacements that were reached during the experiments. Plastic orthotropic material with following properties: modulus of elasticity 68.9 GPa, yield strength 276 MPa, Poisson's ratio 0.33 and density 2700 kg/m3, was used for each model.

Fig. 13 - 15 show the effective plastic strains distributions on the surfaces of the analysed joints. The strains distributions are symmetrical with respect to the X-axis in the specimens with axially-parallel and perpendicular spot welds. In the joints with axially-parallel spots, the concentration of effective plastic strains occurs in the S2 spot welds and the highest value occurs below the weld. In the specimen with perpendicular spots, the concentration zone of effective plastic strains exists base material below the spot welds and the spots edges on the outer sides of the joints. In the joint with eccentrical-parallel spots, the concentration of effective

plastic strains occurs in the S2 spot welds. This distribution is not symmetrical with respect to the X-axis. The higher values are on the right side.
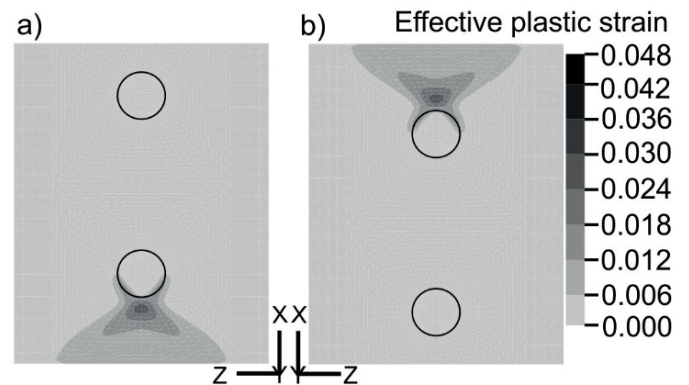

Fig. 13. Results of numerical analysis - effective plastic strains on the surface of specimen with parallel spot welds: a) obverse view, b) reverse view
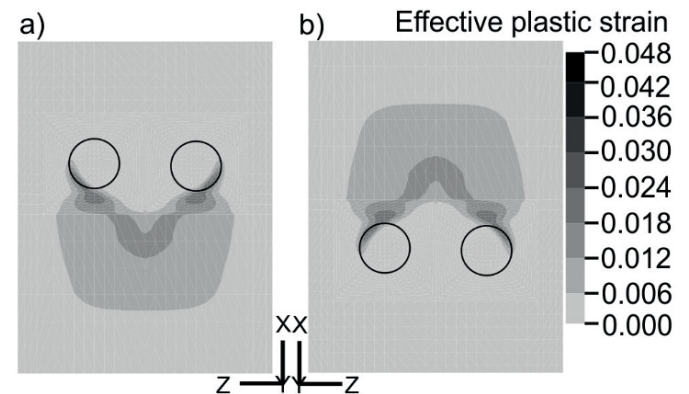

Fig. 14. Results of numerical analysis - effective plastic strains on the surface of specimen with perpendicular spot welds: a) obverse view, b) reverse view
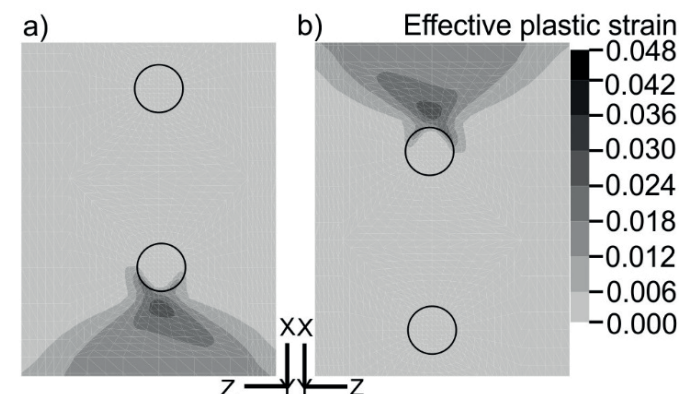

Fig. 15. Results of numerical analysis - effective plastic strains on the surface of specimen with eccentrical, parallel spots: a) obverse view, b) reverse view

The analysis of the effective plastic strains in the numerical models, for each specimen, regardless of the spot weld arrangement, showed that the largest values occur around spot weld edges at joint internal sides.

5. Discussion

The similar values of tensile strength of the joints follow from the adopted space between the spot welds. However the displacement of the s specimen with eccentrical-parallel joints is almost twice as high as the displacement of specimen with the axial-parallel spots.

The optical deformation analysis system allows for the acquisition of effective plastic strain distributions at the selected surfaces of the specimens. The results from the experimental studies are comparable with the specimens from the series, despite manual production of the joints.

Fig. 16 shows the graphs of effective plastic strains along the characteristic lines passing through the maximum of effective plastic strains obtained by the optical measurement system and the numerical analyses.
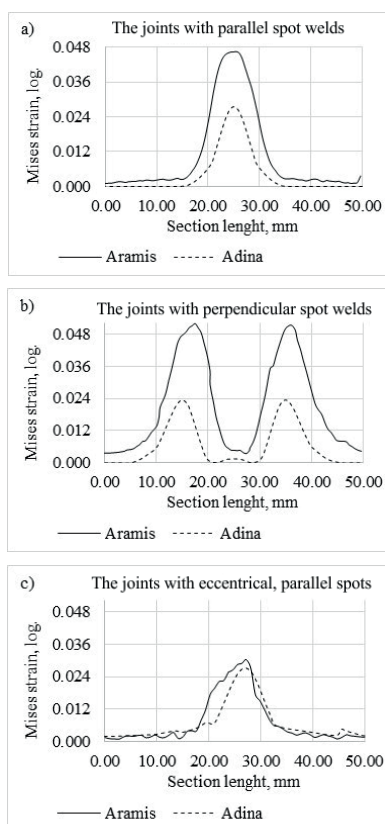

Fig. 16. Graph of effective plastic strains along characteristic lines passing through the maximum effective plastic strains of specimen: a) with parallel spot welds, b) with perpendicular spot welds, c) with eccentrical, parallel spots

The distribution of effective plastic strains concentration areas obtained in numerical analyses is similar to the experimental results. For specimens with parallel spot welds and with perpendicular spot welds quantitative differences amount to about 50%, but the shapes of the distributions in Adina and in Aramis are comparable.

6. Conclusions

- Tensile strength of the specimens with two spots is similar with an average of 18.5 kN.

- In the specimens with parallel spot welds to displacement direction, the joints were destroyed by shearing at the spots.
- In the joint with perpendicular spots to displacement, the spot welds were not destroyed. They were only separated from the base material near the edges, at the sides corresponding to the fixed ends of the sheets. This leads to the loss of joint load capacity.
- The analysis carried out with the optical deformation system does not provide information about the effective plastic strain distribution throughout the specimen volume. It only allows to get results at the selected surface. The combination of optical and numerical analyses allows for determination of the crack location in the whole specimen volume.

REFERENCES

[1] P. Lacki, Z. Kucharczyk, R. E. Śliwa, T. Gałaczyński, Arch. Metall. Mater. 58, 2 (2013).

[2] K. Kudła, K. Wojsyk, Z. Kucharczyk, Met. Form. **3**, 179–191 (2013).

[3] K. Kudła, K. Wojsyk, K. Adamus, Met. Form. **3**, 193-203 (2013).

[4] Y. F. Sun, J. M. Shen, Y. Morisada, H. Fujii, Mater Design. **54**, 450–457 (2014).

[5] K. Kudła, K. Wojsyk, P. Lacki, R. Śliwa (in Polish), Mater. Eng. 5, 306–309 (2009).

[6] T. Sadowski, P. Golewski, E. Zarzeka-Raczkowska, Comp. Mater. Sci. 50, 4, 1256–1262 (2011).

[7] P. Lacki, J. Adamus, T. Sadowski, K. Wojsyk, M. Kneć, in: J. Eberhardsteiner et.al. (Ed.), Vienna, Austria (2012).

[8] T. Sadowski, T. Balawender, R. Sliwa, P. Golewski, M. Knec, Arch. Metall. Mater. **58**, 1 (2013).

[9] P. Lacki, J. Adamus, W. Wieckowski, J. Winowiecka, Arch. Metall. Mater. **58**, 1 (2013).

[10] Z. Shen, X. Yang, S. Yang, Z. Zhang, Y. Yin (en), Mater. Design. **54**, 766–778 (2014).

[11] T. Rosendo, B. Parra, M. Tier, A. da Silva, J.F. dos Santos, T.R. Strohaecker, N.G. Alcântara, Mater. Design. **32**, 3, 1094–1100 (2011).

[12] U. Suhuddin, L. Campanelli, M. Bissolatti, H. Wang, R. Verastegui, J.F. dos Santos, in H. Fujii (Ed.), Osaka, Japan 15–21 (2013).

[13] Z. Shen, X. Yang, Z. Zhang, L. Cui, T. Li (en), Mater. Design **44**, 476–486 (2013).

[14] A. da Silva, J.F. dos Santos, T.R. Rosendo, F.D. Ramos, C. Mazzaferro, M. Tier, L. Bergmann, J. Mazzaferro, T.R. Strohaecker. Warrendale, PA: SAE International (2007).

[15] P. Lacki, A. Derlatka, Met. Form. **24**, 3, 205–218 (2013).

2591

[16] A. Derlatka, P. Kasza, Adv. Mat. Res. **1020**, 151–157 (2014).

[17] A. Derlatka, P. Kasza, Adv. Mat. Res. **1020**, 158–164 (2014).

[18] M. Assidi, L. Fourment, S. Guerdoux, T. Nelson, Int. J. Mach. Tool. Manu. **50**, 2, 143–155 (2010).

[19] Z. Zhang, H. W. Zhang, J. Mater. Process. Tech. **209**, 1, 241–270 (2009).

[20] J.W. Yoon, G.H. Bray, R. Valente, T. Childs, Thin. Wall. Struct. **47**, 12, 1608–1622 (2009).

[21] P. Fanelli, F. Vivio, V. Vullo, Eng. Fract. Mech. **81**, 17–25 (2012).